Transition from Order to Configurational Disorder for Surface Reconstructions on $SrTiO_3(111)$

L. D. Marks,[1,*] A. N. Chiaramonti,[1,‡] S. U. Rahman,[2] and M. R. Castell[2]
[1]Department of Materials Science and Engineering, Northwestern University, Evanston, Illinois 60208, USA
[2]Department of Materials, University of Oxford, Parks Road, Oxford OX1 3PH, United Kingdom
(Received 15 October 2014; published 2 June 2015)

There is growing interest in ternary oxide surfaces due to their role in areas ranging from substrates for low power electronics to heterogeneous catalysis. Descriptions of these surfaces to date focus on low-temperature explanations where enthalpy dominates, and less on the implications of configurational entropy at high temperatures. We report here the structure of three members of the $n \times n$ $(2 \leq n \leq 4)$ reconstructions of the strontium titanate (111) surface using a combination of transmission electron diffraction, density functional theory modeling, and scanning tunneling microscopy. The surfaces contain a mixture of the tetrahedral TiO_4 units found on the (110) surface sitting on top of octahedral $TiO_5[]$ (where [] is a vacant octahedral site), and TiO_6 units in the second layer that are similar to those found on the (001) surface. We find clear evidence of a transition from the ordered enthalpy-dominated 3×3 and 4×4 structures to a configurational entropy-dominated 2×2 structure that is formed at higher temperatures. This changes many aspects of how oxide surfaces should be considered, with significant implications for oxide growth.

DOI: 10.1103/PhysRevLett.114.226101 PACS numbers: 68.35.B-, 68.37.-d, 68.47.Gh

There is currently substantial interest in the surfaces of strontium titanate for a range of applications such as thin film growth [1,2], as a model system for catalytic applications [3], or as an active catalyst with supported nanoparticles [4,5], and in its use either as a substrate or an active material for oxide electronics (e.g., Refs. [6–11]). Even though strontium titanate is a comparatively simple oxide, the archetype perovskite, its myriad surface structures make most other materials seem rather straightforward. For example, there are a very large number of different reconstructions even on the simple (001) surface [12], many of which remain unsolved. Some details for the titanium-rich reconstructions are now understood as consisting of permutations on TiO_2 double layers. As we point out here, these surfaces can be considered as tilings of octahedral $TiO_5[]$ units, where "[]" denotes a vacant oxygen site, normally in an ordered structure although glasslike disordered structures are also possible [13], in effect a Potts-type model.

Compared to the other low-index terminations, much less is known about the polar $SrTiO_3(111)$ surface. A wide range of reconstructions have been observed depending upon the annealing time (on the scale of hours), temperature, oxygen partial pressure, and whether the specimens were ion beam sputtered before analysis, including (1×1) [14–16], $(9/5 \times 9/5)$ [17–19], $(\sqrt{7} \times \sqrt{7}R19.1°)$ [20], (3×3) [17–19], $(\sqrt{13} \times \sqrt{13}\,R13.9°)$ [20], (4×4) [17–19], (5×5) [19], and (6×6) [17–19] reconstructions, as well as a TiO overgrowth under highly reducing conditions [19]. While the approximate chemistry and topography of the surfaces is relatively well characterized, as are some details of the dependence upon surface composition [21], the actual atomic structure of all these surfaces is completely unknown. A few theoretical studies in the literature focus on relatively simple structures that have not been found experimentally [22–24].

For a system as complicated as this with numerous different reconstructions a subtle question is whether it is describable by the simple $T = 0$ K thermodynamics normally used in density functional theory (DFT) calculations to explain surface structures. It is well known that at elevated temperatures the configurational entropy can dominate for Potts models (e.g., Refs. [25–30]). Using an ideal solution model with a variable TiO_2 excess at the surface, the occupancies of different surface structures can be described as

$$c_i = \frac{\exp(-n_i\{G_i - \mu f_i\}/kT)}{\sum \exp(-n_i\{G_i - \mu f_i\}/kT)}, \tag{1}$$

where c_i is the fraction of each surface phase, G_i is the free energy per 1×1 unit cell, n_i is the number of cells in the surface unit cell, f_i is the TiO_2 excess per 1×1 unit cell, and μ is the TiO_2 surface chemical potential, which is chosen such that $\sum c_i f_i$ is the surface TiO_2 excess per 1×1 cell. With this model the fraction of each surface phase is relatively simple at low temperatures, and should be consistent with $T = 0$ K density functional theory calculations. However, at the elevated temperatures typically used to prepare oxides (near half the melting temperature and above) the surface could be a complicated mixture, in effect a glass having only local order. A full

Potts model analysis would include interaction free energy terms between the different structures and be able to make predictions about domain sizes of reconstructions as a function of temperature.

We show here evidence for this different description of oxide surfaces for the case of the $SrTiO_3(111)$ surface. We report the structure of three members of the $n \times n$ $(2 \leq n \leq 4)$ reconstructions using a combination of transmission electron diffraction, density functional theory modeling, and scanning tunneling microscopy. The surfaces contain tetrahedral TiO_4 units similar to the (110) surface, sitting on top of octahedral $TiO_5[]$, and TiO_6 units in the second layer similar to those found on the (001) surface. However, while the 3×3 and 4×4 structures can be well described as conventional, ordered structures, the 2×2 structure is best described as a configurational glass.

For transmission electron microscopy examination, strontium titanate (111)-oriented single-crystal samples were prepared as described previously [18]. A series of eleven transmission electron diffraction patterns to capture the full dynamic range of intensities for all of the spots for the $n \times n$ surfaces was acquired using a microscope equipped with a thermionic filament. The diffraction data were reduced and symmetry averaged to yield a single list of symmetry-independent intensity data and associated errors.

For the STM work, $SrTiO_3$ single crystal substrates doped with a mass fraction of 0.005 Nb and epi-polished (111) surfaces were grown by SurfaceNet GmbH, Germany. (The identification of commercial products is to specify the experimental conditions and does not imply any NIST endorsement or recommendation that they are necessarily the best for the purpose.) The preparation of the surface reconstructions for STM imaging was carried out in a JEOL JSTM4500 s UHV surface analysis facility [19]. The samples were degassed to remove all contamination, Ar^+ ion sputtered for 6 min at 0.5 keV, and then annealed. Different annealing temperatures, durations, and O_2 partial pressures resulted in different reconstructions. The 4×4 reconstruction was obtained through a 1 h anneal at 1000 °C in UHV conditions. The 3×3 reconstruction was obtained following a 5 h anneal at 1150 °C in an O_2 partial pressure of 4.5×10^{-4} Pa. The surfaces containing regions of 2×2 reconstruction were obtained following a 5 h anneal at 1280 °C in an O_2 partial pressure of 6×10^{-4} Pa. In all cases the cooling rate was approximately 6 °C/min. Constant current STM images were taken at room temperature using etched tungsten tips. In all cases the surfaces required high biases to image, indicating that none were reduced.

DFT calculations were performed with the all-electron augmented plane wave + local orbitals WIEN2K code [31] with the revTPSS [32] and MS2 [33] functionals, with a 0.5 on-site exact exchange similar to earlier work [13] and an error of approximately 0.05 eV/1×1 cell; more details can be found in the Supplemental Material [34].

Based upon the STM images and by the use of DFT methods we were able to determine the 3×3 structure, and then verify it using the electron diffraction data, which is very sensitive to fine surface structure details in all layers. The 4×4 surface is sufficiently similar to the 3×3 surface that it could then be solved rather directly. With the main structural units for the (111) surface now defined, it was possible to find the 2×2 surface structure via DFT, checking with STM simulations. For completeness, additional experiments using aberration-corrected plan-view imaging were performed, and while these were consistent with the 3×3 structure described below, they were not definitive and are not discussed further here.

We will first describe the ordered 3×3 and 4×4 structures as these provide the main clues to the intrinsically disordered 2×2 structure. The main results are shown in Figs. 1 and 2, respectively. For the 3×3 structure with 94 symmetry reduced intensities, using just the top titanium and oxygen atoms (six atoms, 12 positions, and one temperature factor) gave an $R1 = 0.37$ $\chi = 2.7$, while including the 2nd-layer atoms (11 atoms, 22 variables, and one temperature factor) gave an $R1 = 0.22$ $\chi = 2.0$, a good fit to the experimental diffraction data (see Table S1 and Fig. S1 in the Supplemental Material [34]). For the 4×4 structure the experimental diffraction data were not very good (large errors associated with weak and overlapping spots as well as dynamical artifacts), and with the presence of twinning there are too many ambiguities for a structural refinement. These surfaces are paradoxically both complicated and simple, and can be described in terms of a second layer of $TiO_5[]$ or TiO_6 octahedral units capped with a sixfold ring of TiO_4 tetrahedra with a face outwards towards vacuum with linear connections of TiO_4 tetrahedra with an edge outwards to vacuum. As found for other oxide reconstructions [41], bond-valence sums indicate that all the titanium atoms are close to their nominal 4^+ valence, and the oxygen similarly with 2^- valence, consistent with a dominance of local bonding in the energetics and similarities to bulk oxides. The DFT refined structures are provided as crystallographic information files (CIF) in the Supplemental Material [34].

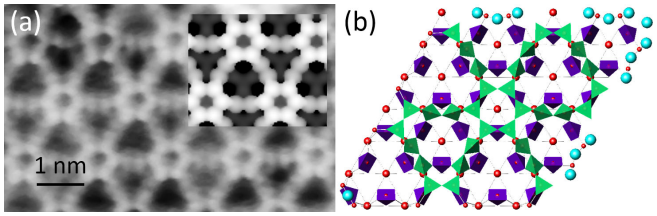

FIG. 1 (color online). (a) Raw STM image (+2.0 V sample bias, 0.38 nA tunneling current) of the 3×3 structure with a simulation inserted on the top right and (b) diagram of the structure with $TiO_5[]$ octahedra purple, TiO_4 tetrahedra green, and Sr atoms red. More details of the structure are in the CIF in the Supplemental Material [34].

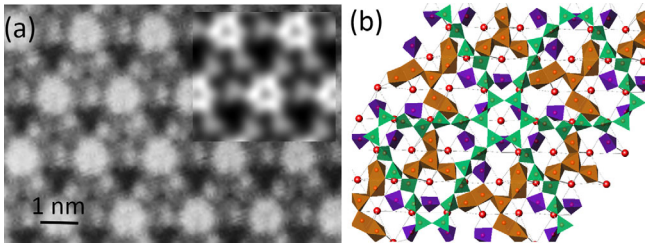

FIG. 2 (color online). (a) Raw STM image (+2.0 V sample bias, 0.50 nA tunneling current) of the 4×4 structure with a simulation inserted on the top right and (b) diagram of the structure with TiO_6 octahedra brown, TiO_5[] octahedra purple, TiO_4 tetrahedra green, and Sr red. More details are in the CIF in the Supplemental Material [34].

Very different from the 3×3 and 4×4 structures, we observed only localized ordered regions in the STM images that had 2×2 cells. Careful analysis allowed us to identify at least two structural units, which are shown in Fig. 3. The first has threefold symmetry and is a partial ring of TiO_6 or TiO_5[] units; the second contains tetrahedral units similar to the 3×3 and 4×4 structures, but now in more linear arrangements and is strictly a $c\left(\begin{smallmatrix}1 & 0\\ 1 & 2\end{smallmatrix}\right)$ structure. For completeness, the symmetry breaking is not a consequence of irregularities in the STM tip, and was locally reproducible between scans (see Fig. S2 in the Supplemental Material [34]).

We note that the degree of enrichment in TiO_2 for the 2×2, 3×3, and 4×4 structures matches expectations based upon how they were prepared. The dominant cation defect in strontium titanate is a strontium vacancy, and at higher temperatures these will diffuse away from the surface leading to a lower TiO_2 surface excess as we found with $4 \times 4 > 3 \times 3 > 2 \times 2$ in the reverse order of the temperatures at which they were annealed.

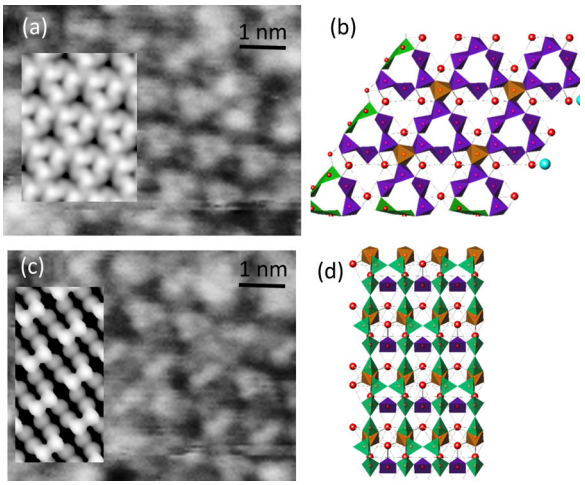

FIG. 3 (color online). (a) Raw STM image (+2.0 V sample bias, 0.37 nA tunneling current) of a $p3$ $2 \times 2a$ structure with a simulation inserted on the left and (b) diagram of the structure with TiO_6 octahedra brown, TiO_5[] octahedra purple, TiO_4 tetrahedra green, and Sr red. More details are in the CIF file. (c) A lower symmetry $2 \times 2b$ structure (strictly the $c\left(\begin{smallmatrix}1 & 0\\ 1 & 2\end{smallmatrix}\right)$) region that coexisted with the $p3$ structure, with a STM simulation (inset) and the structure in (d). Details of the structures are in the CIF in the Supplemental Material [34].

With the knowledge that the 3×3 and 4×4 structures have tetrahedral or octahedral arrangements, a more complete analysis was performed via DFT calculations of more than 120 different structures to understand the 2×2 surface, summarized only for the structures near the convex hull in Fig. 4, with details of the surface enthalpies also available in Table S2 and the CIF in the Supplemental Material [34]. From this we were able to identify a potentially stable low-TiO_2 endpoint for a linear arrangement of TiO_4 *and* TiO_5[] units (labeled Low in Fig. 4) as well as a high coverage two-dimensional arrangement of the same units (labeled High in Fig. 4), see also Fig. S3 in the Supplemental Material [34]. In addition to these and the other structures described above, there were also a large number of permutations of essentially the same units. Within the accuracy of the functionals the DFT convex hull is consistent with the experimental results.

It was unexpected that the energies of all the structures from the 2×2 to the high-coverage structure lie very close to a straight line, which has some significant implications to which we now turn, keeping in mind information we know from the (001) and (110) surfaces. The (001) surface is dominated by arrangements of edge- or corner-shared TiO_5[] units to yield a valence-compensated structure, exactly which are formed depending heavily upon the kinetics during sample preparation [42,43], as well as the surface composition, with both ordered and glasslike disordered structures possible. More formally, except for the 2×1 structure, all the (001) reconstructions can be

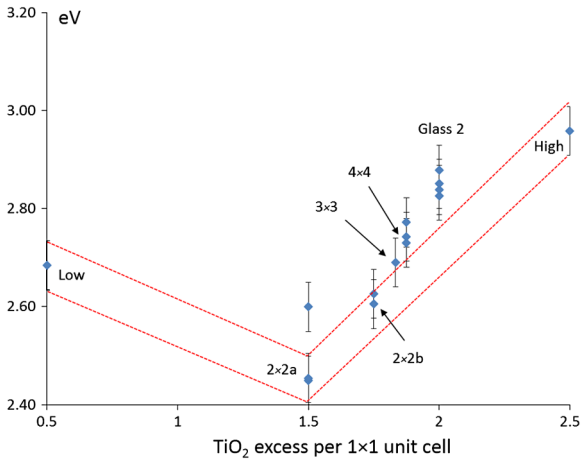

FIG. 4 (color online). Convex hull for the revTPSS results with the x axis the TiO_2 excess per 1×1 surface unit cell and the y axis the surface enthalpy in eV per 1×1 surface unit cell. More details can be found in Table S2 and the CIF in the Supplemental Material [34].

considered via a constrained Ising model. For any lattice site above a second-layer oxygen, the analogue of "spin up" is a planar TiO_4 unit, and of "spin down" a vacancy with the constraints that all oxygen atoms in the outermost layer are bonded to two or more titanium atoms and the total composition is valence neutral—see Fig. S4 in the Supplemental Material [34].

Similarly, the (110) $n \times 1$ reconstructions have a bulk layer terminated by a valence-compensated arrangement of TiO_4 corner-shared tetrahedral units forming ring structures as well as a homologous series of reconstructions [44]. These can be represented as a constrained Potts model with a higher degree of freedom corresponding to placing one of the two types of tetrahedral units either above an oxygen in the second layer or bridging, with a similar valence neutrality condition—see Fig. 2 in Ref. [44].

On the (111) surface the 3×3 and 4×4 structures are more complicated Potts variants with $TiO_5\square$ or TiO_6 octahedral units in the second layer and tetrahedral units very similar to the (110) surface in the outer surface. If we compare these to the other structures in the convex hull, they contain combinations of the same types of units with bridging TiO_4 units either between two oxygens on different $TiO_5\square$ units or two oxygens on one TiO_6 unit as in the $c\left(\begin{smallmatrix}1 & 0\\ 1 & 2\end{smallmatrix}\right)$ structure in Fig. 3, and in a few cases Sr atoms within the structure.

Since the different structures all lie on essentially a straight line in the enthalpy-coverage convex hull of Fig. 4, for any specific surface excess of TiO_2 there will be many different mixtures of structures with nearly degenerate enthalpies. A prediction of the Potts model applied to surfaces is that at elevated temperatures, particularly in the simplified form of Eq. (1), many surfaces will become a complicated mixture of different structural units resulting in small domains of different reconstructions, which is what we have here. At very high temperatures the domains become so small that the surface structure is in effect a glass, with a structure that is driven by the configurational entropy. For instance, there may be rotational glasses as well as coexistence at the nanoscale, such as very small regions of 3×3 structure embedded within areas that have predominantly a 2×2 structure, and this is indeed found experimentally (see Fig. 5). Based upon the experimental results we estimate that a temperature of 1280 °C is sufficient to enter the regime where the configurational entropy terms dominate.

This fundamentally changes how we consider oxide surfaces, with substantial implications for applications in oxide growth, functional electronic materials, as well as catalysis. We need to differentiate between a low-temperature regime, where distinct structures are formed with both long- and short-range order, and a high-temperature regime where the surface has short-range order but long-range disorder. Surfaces rapidly cooled from high temperatures will have a quenched-in disorder, as will

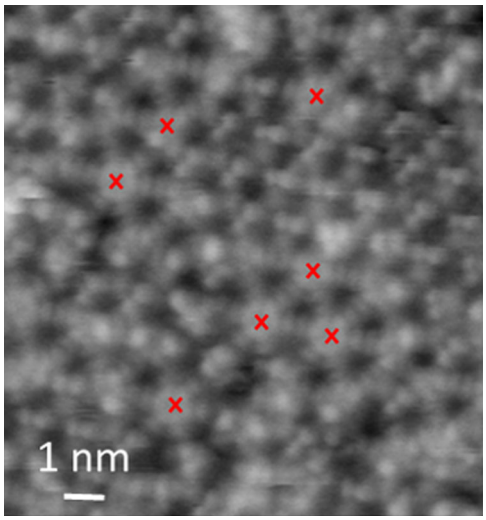

FIG. 5 (color online). STM image (+2.0 V sample bias, 0.38 nA tunneling current) of an area of the dominantly $2 \times 2b$ surface showing a few cells of 3×3 structure embedded in the structure, with the characteristic sixfold ring of the latter marked with red crosses. Note the presence of dumbbells with different orientations, indicative of a rotational glass.

surfaces fabricated by methods such as atomic layer deposition at relatively low temperatures. It is very likely that in many cases the surface structures are formed during cooling rather than at the high temperature soak during the annealing, so slight variations in experimental treatments such as differences in cooling rates can and will lead to very different results. This is entirely consistent with the multitude of structures seen in the literature. Taking this picture one step further, increased configurational disorder is likely to increase the density of domain boundaries and other high-enthalpy local defects, which might have enhanced oxygen exchange rates for fuel cell and other applications such as electrolysis; surface doping to increase the entropy and reduce the disorder temperature is an interesting design concept. This connects to the large body of literature on the importance of surface defects and their local structure for many properties (e.g., Ref. [45]), for instance, reactivity at different surface sites in TiO_2 polymorphs [46] to give just one example.

Ideas such as Potts models for simpler surface phenomena such as chemisorption or melting are well known in the literature (e.g., Refs. [47–52]), but we are not aware of their extension to more complicated oxides as we have done here. There is no reason why this should be limited to just oxides; in fact, hydroxides are probably very similar as suggested by earlier work on MgO and NiO hydroxylated surfaces [53,54].

In summary, by a combination of STM, transmission electron microscopy, and DFT we have determined the structure of the 2×2, 3×3 and 4×4 reconstructions on the strontium titanate (111) surface. While the 3×3 and 4×4 structures are relatively straightforward structures,

the 2×2 structure is a much more complicated mixture. The DFT analysis indicates that there are a large number of surface structures all close to the convex hull, a condition that makes the configurational entropy terms very important. Combining these results with knowledge of the (001) and (110) surfaces, we point out that these oxide surfaces can all be described in a general framework of Ising or Potts models with short-range order but not necessarily long-range order. This not only changes the framework within which we need to consider these surfaces, but opens the door to new ideas to design oxide surfaces by deliberately manipulating the degree of long-range order by changing thermal treatments or doping to force changes in the configurational entropy.

The authors would like to acknowledge Mark Asta and Axel Van Der Waals for useful discussions on ordering, as well as James Ciston, Peter Stair, and Kenneth Poeppelmeier during the course of the work and Peter Blaha for a prerelease version of the code to calculate the MS2 meta-GGA functional. L. D. M. acknowledges funding by both the U.S. National Science Foundation under Grant No. 1419195 and the U.S. DOE under Grant No. DE-FG02-01ER45945 during the period of this work. A. N. C. acknowledges funding for her prior experimental work from the Northwestern University Institute for Catalysis in Energy Processes (ICEP) under Grant No. DOE DE-FG02-03-ER15457. This work is a partial contribution of NIST, an agency of the U.S. Government, and therefore is not subject to copyright in the United States.

*Corresponding author.
l-marks@northwestern.edu
‡Present address: Applied Chemicals and Materials Division, Material Measurement Laboratory, National Institute of Standards and Technology, Boulder, Colorado 80305, USA.

[1] A. Ohtomo, D. A. Muller, J. L. Grazul, and H. Y. Hwang, Nature (London) **419**, 378 (2002).
[2] A. Ohtomo and H. Y. Hwang, Nature (London) **427**, 423 (2004).
[3] Y. Lin, J. Wen, L. Hu, R. M. Kennedy, P. C. Stair, K. R. Poeppelmeier, and L. D. Marks, Phys. Rev. Lett. **111**, 156101 (2013).
[4] J. A. Enterkin, K. R. Poeppelmeier, and L. D. Marks, Nano Lett. **11**, 993 (2011).
[5] J. A. Enterkin, W. Setthapun, J. W. Elam, S. T. Christensen, F. A. Rabuffetti, L. D. Marks, P. C. Stair, K. R. Poeppelmeier, and C. L. Marshall, ACS Catal. **1**, 629 (2011).
[6] J. Mannhart and D. G. Schlom, Science **327**, 1607 (2010).
[7] H. Takagi and H. Y. Hwang, Science **327**, 1601 (2010).
[8] Z. Yang, C. Y. Ko, and S. Ramanathan, Annu. Rev. Mater. Res. **41**, 337 (2011).
[9] P. Zubko, S. Gariglio, M. Gabay, P. Ghosez, and J. M. Triscone, Annu. Rev. Condens. Matter Phys. **2**, 141 (2011).
[10] H. Y. Hwang, Y. Iwasa, M. Kawasaki, B. Keimer, N. Nagaosa, and Y. Tokura, Nat. Mater. **11**, 103 (2012).
[11] J. M. Rondinelli, S. J. May, and J. W. Freeland, MRS Bull. **37**, 261 (2012).
[12] D. T. Newell, *The Surface Structure and Reconstructions of $SrTiO_3$ (001)* (University of Oxford, Oxford, UK, 2007).
[13] D. M. Kienzle, A. E. Becerra-Toledo, and L. D. Marks, Phys. Rev. Lett. **106**, 176102 (2011).
[14] S. Sekiguchi, M. Fujimoto, M. Nomura, S. B. Cho, J. Tanaka, T. Nishihara, M. G. Kang, and H. H. Park, Solid State Ionics **108**, 73 (1998).
[15] Y. Haruyama, Y. Aiura, H. Bando, Y. Nishihara, and H. Kato, J. Electron Sepectrosc. Rel. Phenom. **88**, 695 (1998).
[16] A. Gomann, K. Gomann, M. Frerichs, Kempter, G. V. Borchardt, and W. Maus-Friedrichs, Appl. Surf. Sci. **7**, 2053 (2005).
[17] A. N. Chiaramonti, *Structure and Thermodynamics of Model Catalytic Oxide Surfaces* (Northwestern, Evanston, USA, 2005).
[18] A. N. Chiaramonti, C. H. Lanier, L. D. Marks, and P. C. Stair, Surf. Sci. **602**, 3018 (2008).
[19] B. C. Russell and M. R. Castell, J. Phys. Chem. C **112**, 6538 (2008).
[20] B. C. Russell and M. R. Castell, Phys. Rev. B **75**, 155433 (2007).
[21] J. G. Feng, X. T. Zhu, and J. D. Guo, Surf. Sci. **614**, 38 (2013).
[22] A. Pojani, F. Finocchi, and C. Noguera, Surf. Sci. **442**, 179 (1999).
[23] A. Pojani, F. Finocchi, and C. Noguera, Appl. Surf. Sci. **142**, 177 (1999).
[24] L. D. Marks, A. N. Chiaramonti, F. Tran, and P. Blaha, Surf. Sci. **603**, 2179 (2009).
[25] R. B. Potts, Proc. Cambridge Philos. Soc. **48**, 106 (1952).
[26] F. Y. Wu, Rev. Mod. Phys. **54**, 235 (1982).
[27] D. J. Gross, I. I. Kanter, and H. Sompolinsky, Phys. Rev. Lett. **55**, 304 (1985).
[28] K. Binder and A. P. Young, Rev. Mod. Phys. **58**, 801 (1986).
[29] T. R. Kirkpatrick and P. G. Wolynes, Phys. Rev. B **36**, 8552 (1987).
[30] C. K. Hu, Chin. J. Phys. **52**, 1 (2014).
[31] P. Blaha *et al.*, *WIEN2K, An Augmented Plane Wave Plus Local Orbitals Program for Calculating Crystal Properties* (Technical Univ, Vienna, 2001).
[32] V. N. Staroverov, G. E. Scuseria, J. Tao, and J. P. Perdew, J. Chem. Phys. **119**, 12129 (2003).
[33] J. W. Sun, B. Xiao, Y. Fang, R. Haunschild, P. Hao, A. Ruzsinszky, G. I. Csonka, G. E. Scuseria, and J. P. Perdew, Phys. Rev. Lett. **111**, 106401 (2013).
[34] See Supplemental Material at http://link.aps.org/supplemental/10.1103/PhysRevLett.114.226101, which includes Refs. [35–40] for more details.
[35] J. Tersoff and D. R. Hamann, Phys. Rev. Lett. **50**, 1998 (1983).
[36] L. D. Marks, J. Chem. Theory Comput. **9**, 2786 (2013).
[37] J. P. Perdew, A. Ruzsinszky, G. I. Csonka, O. A. Vydrov, G. E. Scuseria, L. A. Constantin, X. L. Zhou, and K. Burke, Phys. Rev. Lett. **100**, 136406 (2008).
[38] N. Erdman, O. Warschkow, M. Asta, K. R. Poeppelmeier, D. E. Ellis, and L. D. Marks, J. Am. Chem. Soc. **125**, 10050 (2003).

[39] O. Warschkow, M. Asta, N. Erdman, K. R. Poeppelmeier, D. E. Ellis, and L. D. Marks, Surf. Sci. **573**, 446 (2004).
[40] D. M. Kienzle, A. E. Becerra-Toledo, and L. D. Marks, Phys. Rev. Lett. **106**, 176102 (2011).
[41] J. A. Enterkin, A. E. Becerra-Toledo, K. R. Poeppelmeier, and L. D. Marks, Surf. Sci. **606**, 344 (2012).
[42] A. E. Becerra-Toledo, J. A. Enterkin, D. M. Kienzle, and L. D. Marks, Surf. Sci. **606**, 791 (2012).
[43] A. E. Becerra-Toledo, M. R. Castell, and L. D. Marks, Surf. Sci. **606**, 762 (2012).
[44] J. A. Enterkin, A. K. Subramanian, B. C. Russell, M. R. Castell, K. R. Poeppelmeier, and L. D. Marks, Nat. Mater. **9**, 245 (2010).
[45] *Defects at Oxide Surfaces*, edited by J. Jupille and G. Thornton (Springer International Publishing, New York, 2015), Vol. 58, p. 462.
[46] W. K. Li, X. Q. Gong, G. Lu, and A. Selloni, J. Phys. Chem. C **112**, 6594 (2008).
[47] K. Binder and D. P. Landau, Surf. Sci. **108**, 503 (1981).
[48] M. W. Conner and C. Ebner, Phys. Rev. B **36**, 3683 (1987).
[49] C. S. Jayanthi, Phys. Rev. B **44**, 427 (1991).
[50] M. A. Zaluskakotur, Surf. Sci. **265**, 196 (1992).
[51] C. Dobrovolny, L. Laanait, and J. Ruiz, J. Stat. Phys. **116**, 1405 (2004).
[52] C. Dobrovolny, L. Laanait, and J. Ruiz, J. Stat. Phys. **114**, 1269 (2004).
[53] J. Ciston, A. Subramanian, D. M. Kienzle, and L. D. Marks, Surf. Sci. **604**, 155 (2010).
[54] J. Ciston, A. Subramanian, and L. D. Marks, Phys. Rev. B **79**, 085421 (2009).